Journal of The Electrochemical Society, **159** (4) H460-H466 (2012)
0013-4651/2012/159(4)/H460/7/$28.00 © The Electrochemical Society

Stress Gradient Modification of the Electroplated Ni-Diamond Nanocomposite for MEMS Fabrication

Yi-Chia Lee,[a] Yu-Ting Cheng,[b,z] and Wensyang Hsu[a]

[a]*Department of Mechanical Engineering and* [b]*Microsystems Integration Laboratory, Department of Electronics Engineering, National Chiao Tung University, Taiwan 30010, Taiwan, R.O.C.*

The paper investigates the formation of stress gradient in electroplated Ni-based nanocomposite films and presents a process scheme to effectively reduce the stress by lowering plating current density. The stress gradient is characterized by measuring the radius of curvature from the surface profile of Ni-based micro-cantilever beams. For the case of the Ni-based films plated with the current density from 15.3 down to 0.8 mA/cm^2, the stress gradient of the films is formed in the range of −7.13 to −3.23 MPa/μm. According to the cross sectional SEM images, it is found that the Ni-based film plated with 0.8 mA/cm^2 can have a uniformly distributed grain size that can result in a lower stress gradient. By lowering the plating current density from 15.3 to 0.8 mA/cm^2, about 41% and 21% of the stress gradient reduction can be realized in the Ni and Ni-diamond nanocomposite films, respectively, which can be utilized for MEMS resonator fabrication without having structural warpage. Furthermore, experimental results show that the performance of the Ni-diamond nanocomposite resonator can be enhanced in terms of the increase of resonant frequency and quality factor.
 [DOI: 10.1149/2.002205jes]

Manuscript submitted November 21, 2011; revised manuscript received January 12, 2012. Published February 10, 2012.

As a micromechanical structural material, electroplated Ni has drawn many research attentions in MEMS manufacture since it has the characteristics of high deposition rate, low process temperature, low manufacture cost, good electrical conductivity, and high mechanical strength, very suitable for post-CMOS MEMS fabrication.[1,2] A variety of high performance Ni-based MEMS micro-actuators have been demonstrated, such as the electro-thermal actuators with large output displacement for low power applications[3,4] and the micromechanical resonators with high quality factors for monolithic RF CMOS oscillator fabrication.[1,5] Owing to the intrinsic ferromagnetic property of Ni, Ni-based MEMS devices can be also designed with a magnetic-force-driven function,[6,7] applicable for the use in highly conductive salty solutions usually found in in-vivo biological systems.[8] Using the multiple molding/electroplating technology,[9] 3D Ni-based MEMS structures can be constructed with a high aspect ratio of the structural thickness to width (>100)[10] which can effectively not only increase the sensitivity but also reduce the driving voltage in any capacitive type transducers.[11]

Recently, it has been found that the physical properties of Ni can be further reinforced by incorporating a secondary material such as Al_2O_3, SiC, SiO_2, diamond and Carbon Nanotube (CNT) within itself.[12–15] We previously reported a simple process by adding nano-diamond or CNT nanoparticles into an electroplating bath to fabricate Ni-based nanocomposite electro-thermal micro-actuators.[16,17] With appropriate incorporation of the secondary phase, such as nano-diamond or CNT, the nanocomposite actuator can exhibit superior performance including lower power consumption and larger output displacement due to the increase of Young's modulus, hardness and coefficient of thermal expansion (CTE) of the composite material without sacrificing its intrinsic mechanical reliability.[16,18] The property enhancements have led such electroplated Ni-based nanocomposite films for more MEMS applications, especially in RF MEMS including the fabrication of MEMS switch, resonator and filter components.

Nevertheless, as-electroplated Ni film is usually accompanied with residual stress which would cause significant structural deformation like beam curling and membrane winkling in suspended Ni-based MEMS devices. Figure 1 shows a Ni micromechanical resonator electroplated with the current density of 20 mA/cm^2. The 6 μm-thick as-released structure is warped down severely. Ni-diamond nanocomposite micro-resonators also exhibit a similar behavior. Because of the structural deformation, the Ni-based MEMS device would suffer either the problem of performance mismatch like capacitance mismatch[19] or the problem of performance degradation while the device structure must be made stiffer than the original design to overcome the warpage.[20] Since the incorporation of the secondary phase would aggravate the residual stress problem to become more severe in the Ni-based nanocomposite film,[14] it is still a critical research topic to solve the curling phenomenon in the electroplated Ni structures for future MEMS applications.

From solid mechanics point of view, the structural warpage is mainly caused by the existence of stress gradient in the as-electroplated Ni film. Previously, the existence of stress gradient has been observed and investigated in sputtered films, such as Cr, CrN and TiN.[21–23] The model of grain boundary shrinkage[24] was utilized to explain the formation of stress gradient mainly resulted by the grain evolution in the films.[21] The mean stress (σ_{avg}) in the films could be characterized using a power law, $\sigma_{avg} \sim h^{-p}$, where h is film thickness and p is the scaling exponential factor determined by the dynamics of the growth process.[21] According to the TEM observation,[21] the dependence can be attributed to the increase of the grain size over the thickness of the film where the number of grains per unit length (N) is also a function of the film thickness abided by the same power law, $N \sim h^{-p}$. On the other hand, the stress gradient in the electroplated Ni film has not been investigated systemically yet. Only plating temperature has been identified so far as a key process parameter which can lead to the stress gradient relaxation of the film during the plating because Ni atoms can migrate to relaxed positions.[25] Nevertheless, the Ni film plated at high temperature (over 70°C) is usually accompanied with a high thermal stress level and the inclusion of nonmetallic atoms which would affect the elastic properties of the film.[26] Recently,

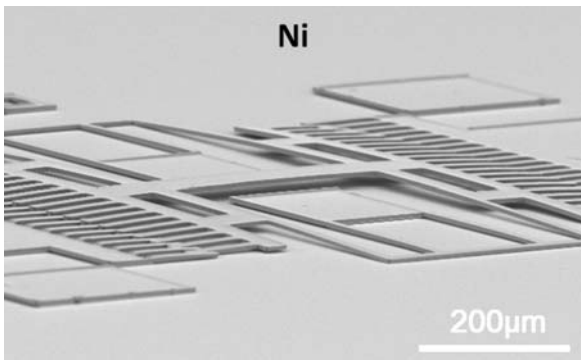

Figure 1. The SEM photograph of Ni comb-typed micro-resonator plated with 20 mA/cm^2.

[z] E-mail: ytcheng@mail.nctu.edu.tw

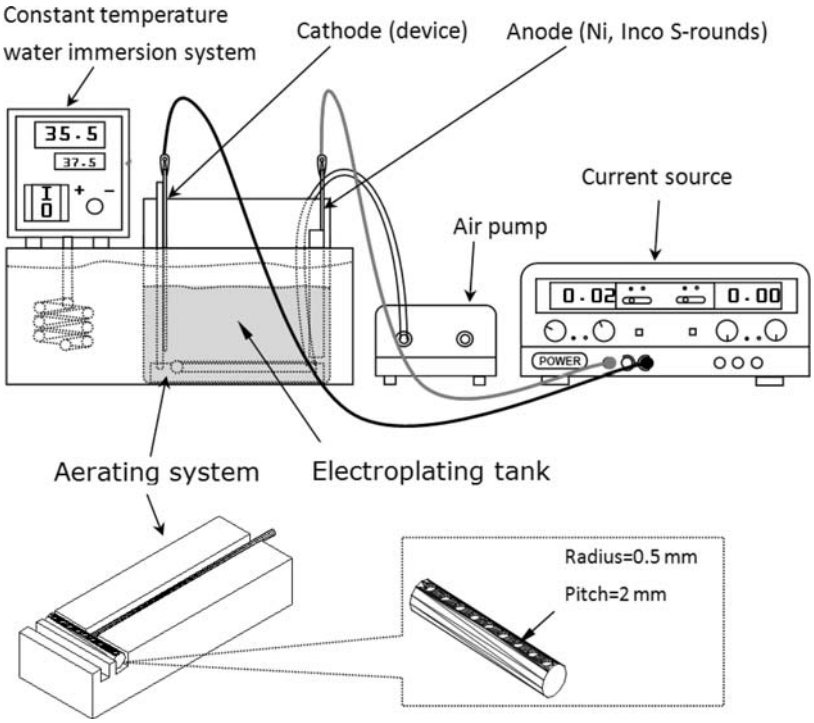

Figure 2. Electroplating system in the work.

it has been reported that the mean tensile stress in electroplated Ni films would also obey the aforementioned power law and the stress level could be reduced by lowering current density.[27] We, therefore, speculate that the formation of the stress gradient in an electroplated Ni film could be resulted by the grain evolution when the film starts growing to become thicker.

Previous investigations have shown that the mean stress in electroplated Ni film could be reduced by current density reduction and the current density will also affect the nucleation and grain growth of the Ni film.[27–29] Thus, in the work, current density effects on the stress gradient of Ni and Ni-diamond nanocomposite films will be investigated and utilized as a process parameter for the modification and reduction of the stress gradient for MEMS fabrication. An optimal plating process with the lowest stress gradient is then derived and utilized to fabricate Ni-based micromechanical resonators. At final, the property enhancement in the nano-diamond-incorporated Ni composite film is verified by characterizing the frequency responses of the micromechanical resonators made of pure Ni and the nanocomposite films, respectively.

Experimental

The preparation of electrolytes.— Sulfamate-based Ni electrolyte is chosen for electroplating due to low residual stress in film deposition. Ni film is DC (direct current) electroplated in the plating bath with the electrolyte comprising of nickel sulfamate of 400 g/L, boric acid of 40 g/L, nickel chloride of 3 g/L, and wetting agent (NPA, Atotech Inc.) of 5 g/L. On the other hand, nano-diamond particles with 125 nm in diameter (Microdiamant AG Co., Ltd.) are added into the electrolyte for electroplating Ni-diamond nanocomposite films. An aerating system as shown in Figure 2 is utilized to increase the diffusion of Ni ions and keep the nano-diamond particles well suspended in the electrolyte. The plating bath with a pH level of $4.1 \sim 4.3$ is put in a tank stored in a water immersion system where the temperature is kept at 35°C. Before being placed into the plating bath, the device substrate is first dipped in a 5% sulfate acid water solution for 10 sec. and then rinsed in de-ionized water for 5 min.

Stress gradient characterization.— Figure 3 shows a micro-cantilever with two kinds of residual stresses which are mean stress (σ_0) and gradient stress (σ_1), respectively. After releasing the sacrificial layer underneath the cantilever as shown in Figure 3b, the beam tends to be bended owing to the stress gradient resulted by the gradient stress. As shown in Figure 3c, the stress gradient, Γ, can be approximately estimated in a linear distribution as follows,[30,31]

$$\Gamma = \frac{\Delta\sigma}{h} = \frac{2\sigma_1}{h} = \left(\frac{E}{1-\nu}\right)\frac{1}{\rho} \qquad [1]$$

where ρ is the radius of beam curvature and E and ν are the Young's modulus and Poisson ratio of a thin film, respectively. Thus, the curvature of the micro-cantilevers made of the electroplated Ni and Ni-diamond nanocomposite films will be measured by White-Light-Interferometer (FOGALE nanotech Inc.) and used for the characterization of the stress gradient.

Fabrication of micro-cantilevers and micro-resonators.— The micro-resonator fabrication starts with photoresist (PR) spin-coating and lithographically patterning on an electrical isolation layer, 500 nm thick SiO_2, followed by Ti/Ni layer (20/200 nm) deposition for device electrode fabrication on a silicon substrate. Sacrificial layer, like PR, is then coated, defined, and deposited with a sputtered Cu seed layer (200 nm) for following Ni-based composite electroplating. Before electroplating the Ni, thick PR like AZ-10XT is spun and patterned on the substrate as a mold (10 μm) where Ni-based film (6 μm) is electroplated to form a microstructure. Micro-resonator fabrication is then finished after the removal of PR mold, Cu seed layer, and sacrificial layer by acetone, the mixture of CH_3COOH and H_2O_2, and PR stripper, respectively. For the case of micro-cantilever, there is no need to fabricate the electrode underneath the beam for the curvature measurement, so the process steps of Ti/Ni layer (20/200 nm) deposition and patterning are skipped.

Characterization of micro-resonators.— Comb-typed micro-resonators are utilized to demonstrate the optimal process with stress gradient reduction and the resonant frequency enhancement based on the improvement of Young's modulus-to-density ratio.[18] The frequency response of the micro-resonators is measured by MEMS Motion Analyzer (Etec Inc., MMA G2) with submicron resolution. The V_{bias} (DC voltage) and V_i (AC voltage) are applied on the fixed

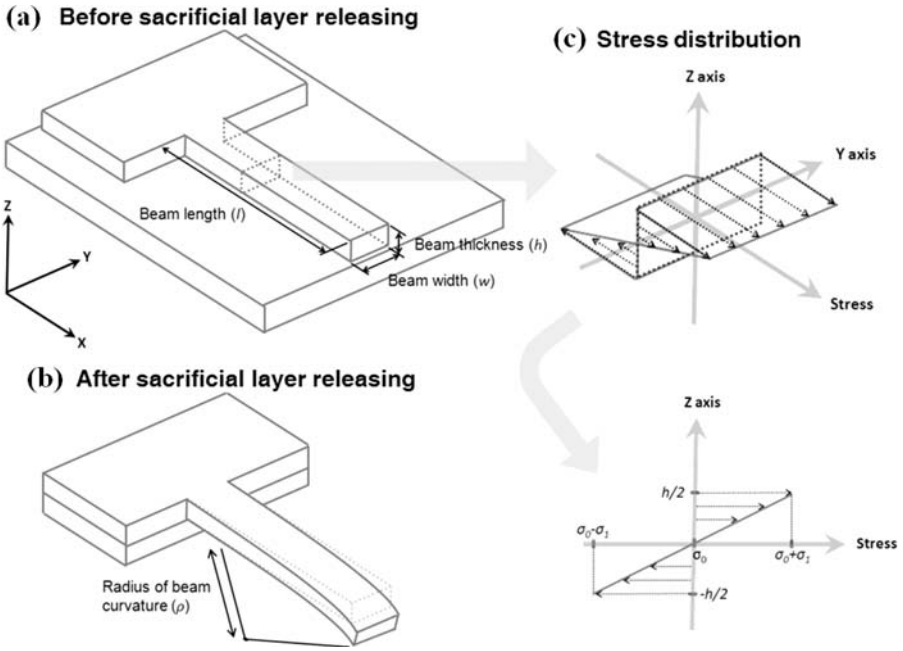

Figure 3. Micro-cantilever beam (a) before and (b) after release. (c) The stress distribution can be expressed by the mean stress (σ_0) and gradient stress (σ_1).

comb-electrode and the resonating structure, respectively and the motion images at different frequency can be synchronously captured by the optical system of the MMA. According to the image data captured at different frequency, the frequency response of the micro-resonator can be obtained with different vibrating amplitude.

Results and Discussion

Stress gradient characterization.— The perpendicular deformation can be resulted by the gradient stress and mean stress.[31] The mean and gradient stresses would cause the beam tilting at its fixed end and the beam curling, respectively. Previously, the mean stress of Ni and Ni-diamond films has been characterized by a long-short beam[32] and the results indicated that both mean stresses are small, which are 6.38 and 7.39 MPa for Ni and Ni-diamond films plated with 15.3 mA/cm^2, respectively, and only result in a few nanometers deformation at the free end of the beam. Since the mean stress would be reduced with the current density reduction,[27] we will neglect the deformation caused by the mean stress in the investigation. Figure 4a and 4b show as-fabricated Ni and Ni-Diamond micro-cantilevers after the sacrificial layer removal. The surface profile of the micro-cantilevers is measured and the associated curvature is then extracted by profile fitting, as shown in Figure 4c and 4d. The Young's moduli of the electroplated Ni and Ni-Diamond nanocomposite films are characterized by nano-indenter (Nano-Indenter XP, MTS systems Co.). On the other hand, the roughness (Ra), thickness, and beam profile of the films are characterized by white-light-interferometer. The measurement results are summarized in Table I. The measured Young's modulus increases with the current density reduction. Both Ni and Ni-diamond nanocomposite films with the plating current density of 7.7 mA/cm^2 can have the lowest surface roughness. Figure 5 shows the correlation between the plating current density versus the stress gradient and deposition rate of electroplated Ni and Ni-diamond

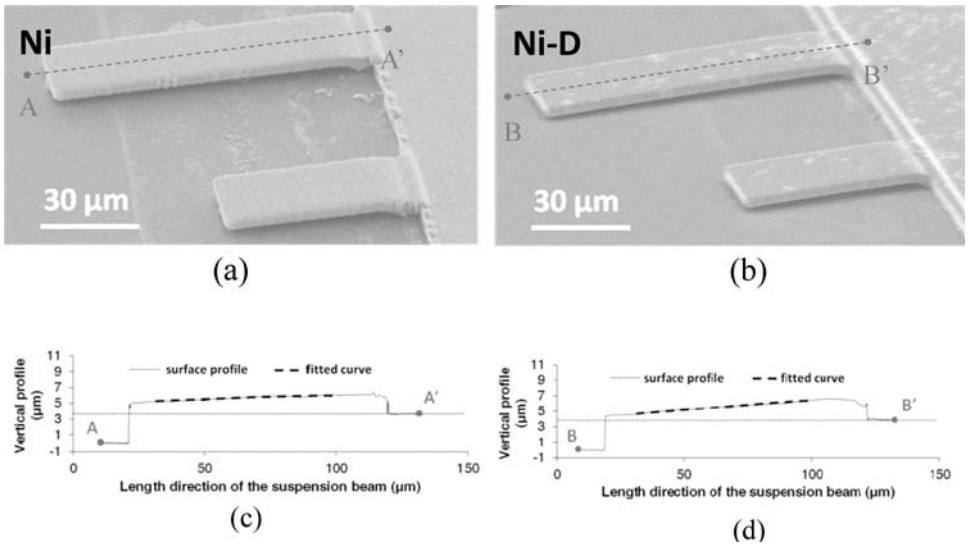

Figure 4. The SEM photographs of (a) Ni and (b) Ni-diamond nanocomposite micro-cantilevers plated with 11.5 mA/cm^2 and White-Light-Interferometer cut views of (a) Ni and (b) Ni-diamond nanocomposite.

Table I. The measured material properties and dimensions of the cantilever beams made of Ni and Ni-diamond nanocomposite.

Units	Current density mA/cm^2	Young's modulus GPa	Roughness nm	Thickness μm	Radius of curvature μm
Ni	15.3	141	23.76	5.34	40230
	11.5	144	41.88	5.85	43853
	7.7	148	9.42	5.79	47092
	3.8	152	20.7	6.15	53743
	0.8	154	34.44	6.54	65343
Ni-diamond	15.3	186	33.78	5.84	40681
	11.5	191	38.7	6.07	42279
	7.7	197	13.08	5.54	43827
	3.8	202	26.04	6.16	44999
	0.8	206	36.48	6.3	52724

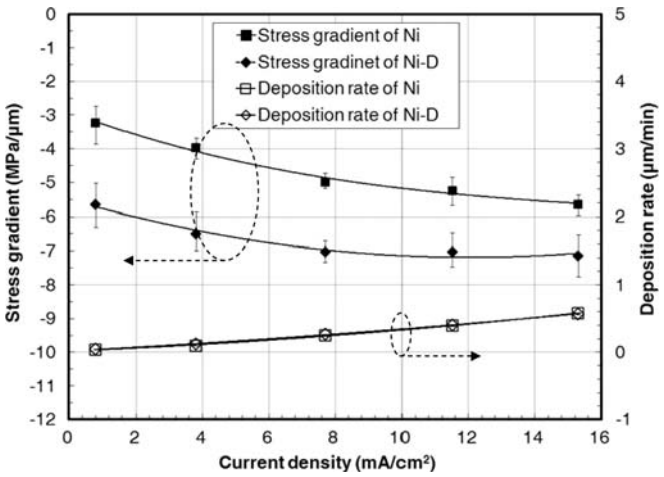

Figure 5. The stress gradient and deposition rate of Ni and Ni-diamond nanocomposite films under different current density.

nanocomposite films. Although the deposition rate of Ni and Ni-diamond nanocomposite films both increases with the increase of plating current density, it is inevitable to have a warped structure while the films are electroplated with high current density resulting in a large stress gradient. In addition, Ni-diamond nanocomposite film has a higher stress gradient than the Ni one. For the same plating current density, the stress gradient of Ni-diamond nanocomposite film is about 1.5 times larger than that of Ni film. By lowering plating current density form 15.3 to 0.8 mA/cm^2, the stress gradient can have 41% (from −5.46 to −3.23 MPa/μm) and 21% (from −7.13 to −5.65 MPa/μm) reduction in Ni and Ni-diamond nanocomposite films, respectively.

From the focused ion beam (FIB) images shown in Figure 6a, it is found that the Ni film plated with higher current density is comprised of finer grains. On the contrary, the average grain size of the Ni film plated with 0.8 mA/cm^2 is larger than the one plated with 15.3 mA/cm^2. As aforementioned, the grain structures in a sputtered polycrystalline film would gradually evolve from the nucleation/seed layer at a fine grain state to a texture structure with a preferred growth direction and the evolution would accompany with the variation of grain size and non-uniform residual stress distribution.[21–23] Figure 7 shows the grain size near the seed layer is about 50 nm. The Ni and Ni-diamond nanocomposite films plated with a lower current density

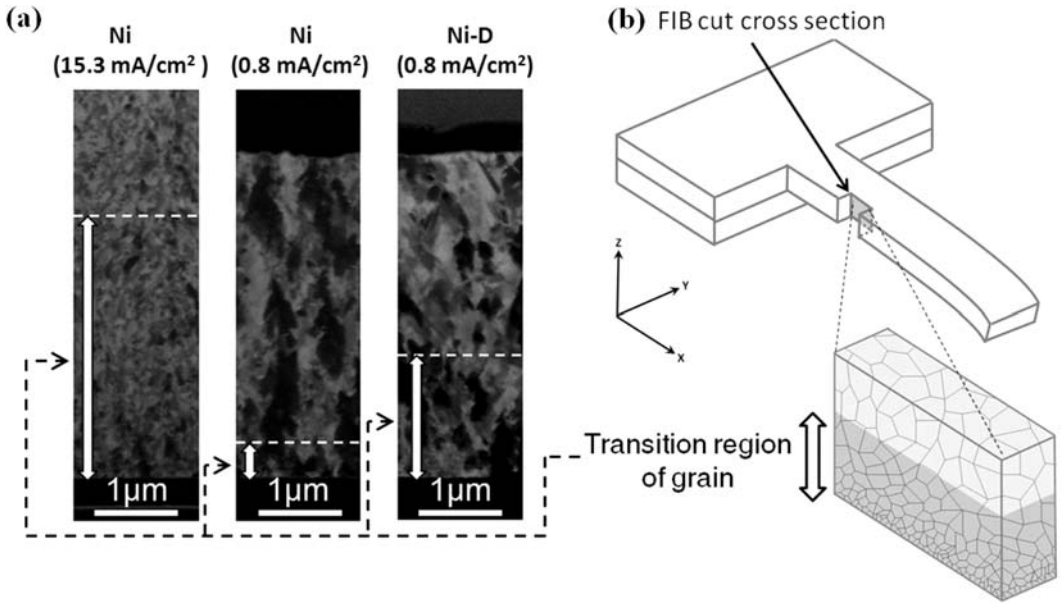

Figure 6. (a) FIB cross sectional images of Ni plated with 15.3 mA/cm^2 and 0.8 mA/cm^2 and Ni-diamond nanocomposite with 0.8 mA/cm^2. (b) Model of grain evolution of electroplated Ni.

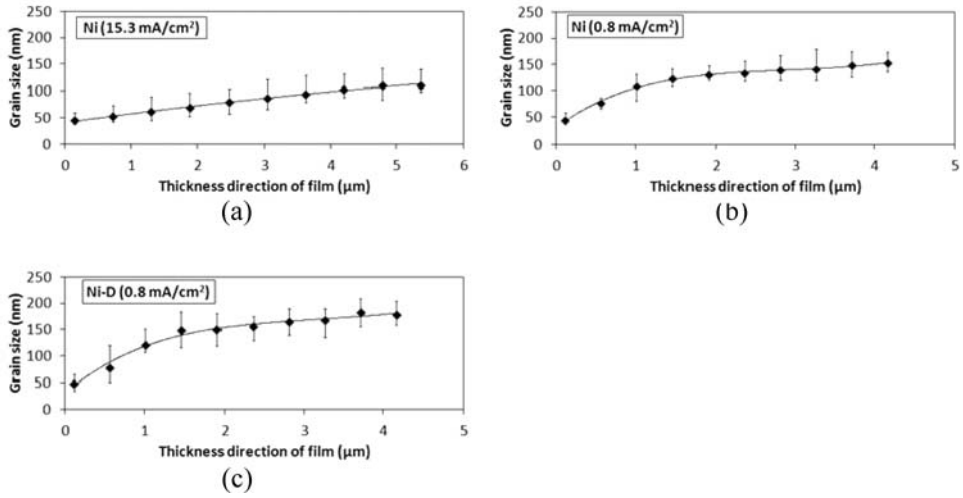

Figure 7. The grain size versus height: Ni plated with (a) 15.3 mA/cm^2 and (b) 0.8 mA/cm^2. (c) Ni-diamond nanocomposite plated with 0.8 mA/cm^2.

would have the grain size distribution quickly saturated with a stable value, i.e. 170 nm and 150 nm in Figure 7b and 7c, respectively. On the contrary, the grain size of the pure Ni one plated with a higher current density would increase with the height along the film thickness and no size saturation is observed as shown in Figure 7a. Thus, for the case of electroplated Ni film, the stress gradient would form in the Ni film while the grain evolution takes place and the film plated with higher current density will exhibit a larger stress gradient resulted by a thicker transition region, i.e. grain variance region, as shown in Figure 6a. In addition, the nanocomposite film plated with 0.8 mA/cm^2 has a grain size distribution similar to the Ni film even though nano-diamond particles are incorporated.

The stress gradient reduction scheme in the electroplating Ni film can be further qualitatively illustrated as follows:

The origin of the stress can be illustrated by the model of grain boundary shrinkage,[24]

$$\sigma(z) = \frac{\delta}{G(z)}\left(\frac{E}{1-\nu}\right) \qquad [2]$$

δ and G(z) are the shrinkage of the grain boundary and the grain size, respectively. Considering a transition region with the thickness of h, the stress gradient (Γ) of the film can be derived and expressed as follows by substituting Eq. 2 into Eq. 1,

$$\Gamma = \frac{\Delta\sigma}{h} = -\frac{\delta E}{1-\nu}\cdot\frac{\Delta G}{h}\cdot\frac{1}{G(z_1)G(z_0)} \qquad [3]$$

where z_0 and z_1 are the location at the bottom and top surfaces of the transition region, respectively. In this expression, it shows the correlation of stress gradient with the grain size variation (ΔG) and grain size ($G(z)$). Thus, electroplated with lower plating current density, the Ni film can have a larger and uniformly distributed grain size which can effectively result in a lower stress gradient.

Figure 8 shows the SEM photographs of Ni (Figure 8a) and Ni-diamond nanocomposite micro-resonators (Figure 8b) electroplated with 0.8 mA/cm^2. Figure 8c and 8d show the cut-views of the micro-resonators taken by White-Light-Interferometer. It indicates that the

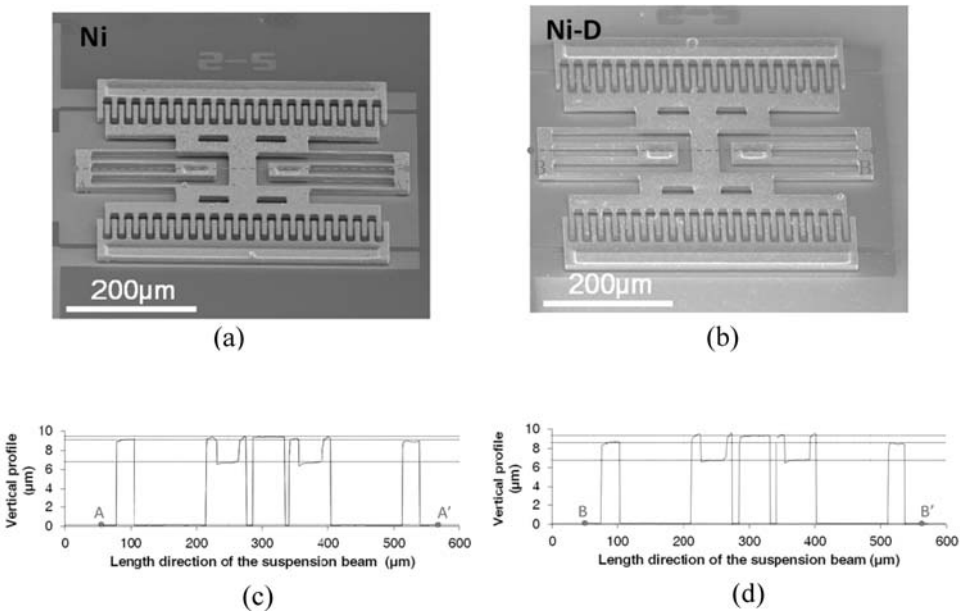

Figure 8. The SEM photographs of (a) Ni and (b) Ni-diamond nanocomposite micro-resonator plated with 11.5 mA/cm^2 and White-Light-Interferometer cut views of (a) Ni and (b) Ni-diamond nanocomposite.

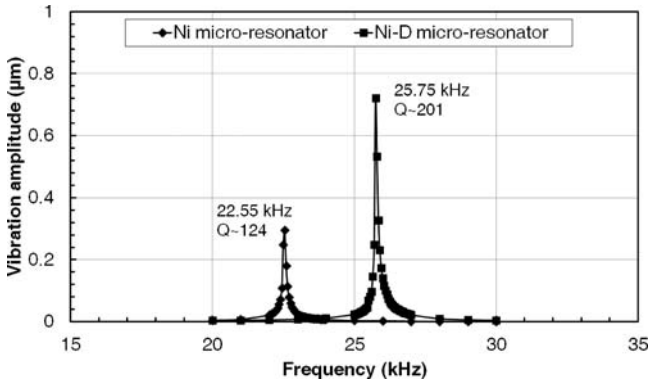

Figure 9. Frequency responses of Ni and Ni-diamond comb-typed micro-resonators at atmospheric pressure.

120 μm long springs still have a little downward warpage but they have been fully suspended to support the whole micro-resonator structures.

Nano-diamond induced performance enhancement of micro-resonator.— Figure 9 shows the frequency response of the micro-resonators made of Ni and Ni-diamond nanocomposite films indicating the related resonant frequencies are 22.55 and 25.75 kHz, respectively. About 14% resonant frequency enhancement can be realized in the Ni-diamond nanocomposite micro-resonator where the composite film is electroplated in a Ni electrolyte with 2 g/L nano-diamonds. Meanwhile, the measured response also shows the Ni-diamond nanocomposite micro-resonator has a higher quality factor than that of Ni at atmospheric pressure. The measured quality factors (Q) of the Ni and Ni-diamond micro-resonators are 124 and 201, respectively, and the damping ratio (ζ) can be derived as follows.

$$Q = \frac{1}{2\zeta} \quad [4]$$

ζ's are 4.03×10^{-3} and 2.49×10^{-3} for Ni and Ni-diamond micro-resonators, respectively.

Thus, by the modal simulation of finite-element-analysis software (Ansys) regarding the frequency responses, the results indicate that the Young's moduli are 144.8 and 187.8 GPa for Ni and Ni-diamond nanocomposite, respectively, which are close to the previously published results.[33] The frequency enhancement can be expected based on the elemental analysis of electroplated nanocomposite film using the tool of elemental analyzer (Heraeus, varioIII-NCH) as shown in Figure 10. From the detected carbon concentration, it is found that the volume percentage of incorporated nano-diamonds is proportion to the nano-diamond concentration in the Ni plating bath. For the nanocomposite film plated in the bath with 2 g/L nano-diamond, the volume

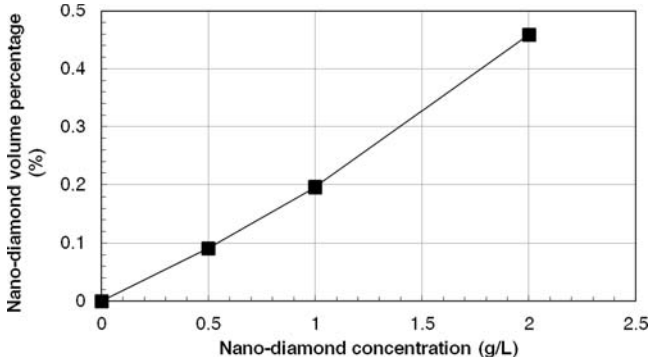

Figure 10. Incorporated nano-diamond volume percentage in the nanocomposite with different nano-diamond concentrations in electrolyte.

percentage of the incorporated nano-diamonds can be increased to 0.46%. According to rule of mixture,[34,35] the Young's modulus of two-phase composite can be estimated by the upper and lower bound expressions as follows, respectively,

$$E_{composite,\,upper} = E_m V_m + E_D V_D \quad [5]$$

and

$$E_{composite,\,lower} = \frac{E_m E_D}{E_m V_D + E_D V_m} \quad [6]$$

where the E_m, E_D, V_m and V_D are Young's moduli and volume fractions of the matrix and secondary phase, respectively. Based on the measured Young's modulus, the mechanical property of the Ni nanocomposite film with the volume ratio of 0.46% nano-diamonds can only have 2.3% and 0.3% Young's modulus enhancements estimated by the upper and lower bounds, respectively. Thus, according to the upper bound of the estimated Young's modulus, it indicates only 1.5% resonant frequency increase can be achieved. In comparison of the measured resonant frequencies of the micro-resonators, nano-diamond incorporation can bring more enhancement than that estimated by the upper bound.

The frequency enhancement can be attributed to two possible factors which can result in the Young's modulus increase of the nanocomposite film. According to the previous study,[36] it was found that the more compressive-stressed film will come with a higher Young's modulus. Since the nano-diamond incorporation would cause Ni film with more compressive stress,[14] it may cause the increase of Young's modulus of Ni part of nanocomposite so that the Young's modulus of the nanocomposite can be enhanced with a value larger than the one estimated by the rule of mixture. Meanwhile, the resonant frequency enhancement can be possibly attributed to more nano-diamond incorporation in the supporting beams of the comb-typed micro-resonators due to limited beam width. Further investigations regarding the stress effect on the mechanical property modification in the Ni matrix and the geometrical effect of the plating mold on the incorporation of nano-diamond in the composite film are, therefore, required for potential MEMS applications.

Conclusions

The stress gradient of electroplated Ni-based films has been well investigated. It is found that the formation of larger Ni grains and smaller grain size variance in the electroplated Ni-based films are the key factors to make the films with small stress gradient which can be controlled by plating current. Experimental results show that 41% and 21% reduction of the stress gradient can be achieved in Ni and Ni-diamond nanocomposite films by lowering the plating current density from 15.3 to 0.8 mA/cm^2, respectively. The structural warpage of as-fabricated MEMS devices can, therefore, be effectively inhibited using lower plating current to make the device itself fully function. About 14% resonant frequency enhancement has been found in the nanocomposite micro-resonators made of the Ni-diamond nanocomposite films plated with the current density of 0.8 mA/cm^2 in the bath containing 2 g/L nano-diamond particles with 125 nm in diameter. The enhancement can be attributed to the increase of Young's modulus/density ratio via the incorporation of nano-diamonds in the Ni matrix. The nanocomposite micro-resonator has shown better device performance including the increase of resonant frequency and quality factor in comparison with the same type of micro-resonator made of electroplated Ni.

Acknowledgments

This work was supported in part by NSC under the Grant 100-2220-E-009-007, NSC 97-2221-E-009-020-MY3, and the Ministry of Education in Taiwan under ATU Program. The authors would like to express the appreciations to Nano Facility Center of National Chiao Tung University and National Chip Implementation Center for the support of the fabrication and measurement instruments.

References

1. W.-L. Huang, Z. Ren, Y.-W. Lin, H.-Y. Chen, J. Lahann, and C. T.-C. Nguyen, in *IEEE 21th International Conference on Micro Electro Mechanical Systems*, pp. 10–13, Tucson, AZ (2008).
2. S. E. Alper, K. M. Silay, and T. Akin, *Sens. Actuators, A*, **132**, 171 (2006).
3. C. P. Hsu and W. Hsu, *J. Microelectromech. Syst.*, **15**, 935 (2006).
4. D. Girbau, L. Pradell, A. Lázaro, and A. Nebot, *J. Microelectromech. Syst.*, **16**, 1061 (2007).
5. W.-L. Huang, Z. Ren, and C. T.-C. Nguyen, in *IEEE International Frequency Control Symposium and Exposition*, pp. 839–847, Miami, FL (2006).
6. D. J. Vasquez and J. W. Judy, in *IEEE 21th International Conference on Micro Electro Mechanical Systems*, pp. 737–741, Tucson, AZ (2008).
7. C. W. Chang and W. Hsu, *J. Micromech. Microeng.*, **19**, 105026 (2009).
8. S. A. Lee, J. R. Pinney, M. Bergsneider, and J. W. Judy, in *the 3rd International IEEE-EMBS Conference on Neural Engineering*, pp. 65–68, Kohala Coast, HI (2007).
9. A. Cohen, G. Zhang, F. G. Tseng, U. Frodis, F. Mansfeld, and P. Will, in *IEEE 12th International Conference on Micro Electro Mechanical Systems*, pp. 244–251, Orlando, FL (1999).
10. K. Kataoka, T. Itoh, T. Suga, and K. Inoue, in *The 50th IEEE Holm Conference on Electrical Contacts*, pp. 231–235, Seattle, WA (2004).
11. S. E. Alper, I. E. Ocak, and T. Akin, *J. Microelectromech. Syst.*, **16**, 1025 (2007).
12. S. L. Kuo, Y. C. Chen, M. D. Ger, and W. H. Hwu, *Mater. Chem. Phys.*, **86**, 5 (2004).
13. L. Orlovskaja, N. Periene, M. Kurtinaitiene, and S. Surviliene, *Surf. Coat. Technol.*, **111**, 234 (1999).
14. K.-S. Teh, Y.-T. Cheng, and L. Lin, *J. Micromech. Microeng.*, **15**, 2205 (2005).
15. T.-Y. Chao, G.-R. Shen, and Y.-T. Cheng, *J. Electrochem. Soc.*, **153**, G98 (2006).
16. L.-N. Tsai, Y.-T. Cheng, W. Hsu, and W. Fang, *J. Vac. Sci. Tech.*, **24**, 205 (2006).
17. C.-S. Huang, Y.-T. Cheng, J. Chung, and W. Hsu, *Sens. Actuators, A*, **149**, 298 (2009).
18. L.-N. Tsai, G.-R. Shen, Y.-T. Cheng, and W. Hsu, *J. Microelectromech. Syst.*, **15**, 149 (2006).
19. S. P. Pacheco, L. P. B. Katehi, and C. T.-C. Nguyen, in *IEEE MTT-S International Microwave Symposium*, pp. 165–168, Boston, MA (2000).
20. D. Peroulis, S. P. Pacheco, K. Sarabandi, and L. P. B. Katehi, in *the 31st European Microwave Symposium*, pp. 173–176, London (2001).
21. G. C. A. M. Janssen, A. J. Dammers, V. G. M. Sivel, and W. R. Wang, *Appl. Phys. Lett.*, **83**, 3287 (2003).
22. G. C. A. M. Janssen, F. D. Tichelaar, and C. C. G. Visser, *J. Appl. Phys.*, **100**, 093512 (2006).
23. R. Machunze and G. C. A. M. Janssen, *Surf. Coat. Technol.*, **203**, 550 (2008).
24. R. W. Hoffman, *Thin Solid Films*, **34**, 185 (1976).
25. J. K. Luo, J. H. He, A. Flewitt, D. F. Moore, S. M. Spearing, N. A. Fleck, and W. I. Milne, *J. Microlithogr. Microfabr. Microsyst.*, **4**, 023012 (2005).
26. J. K. Luo, M. Pritschow, A. J. Flewitt, S. M. Spearing, N. A. Fleck, and W. I. Milne, *J. Electrochem. Soc.*, **153**, D155 (2006).
27. M. Saitou, S. Oshiro, and Y. Sagawa, *J. Appl. Phys.*, **104**, 093518 (2008).
28. A. M. Rashidi and A. Amadeh, *J. Mater. Sci. Technol.*, **26**, 82 (2010).
29. L. Wang, Y. Gao, T. Xu, and Q. Xue, *Mater. Chem. Phys.*, **99**, 96 (2006).
30. S. He, J. S. Chang, L. Li, and H. Ho, *Sens. Actuators, A*, **154**, 149 (2009).
31. W. Fang and J. A. Wickert, *J. Micromech. Microeng.*, **6**, 301 (1996).
32. C. S. Pan and W. Hsu, *J. Microelectromech. Syst.*, **8**, 200 (1999).
33. C.-S. Huang, Y.-T. Cheng, C.-J. Yeh, H.-K. Liu, and W. Hsu, in *the 15th International Conference on Solid-State Sensors, Actuators and Microsystems*, pp. 180–183, Denver, CO (2009).
34. C.-L. Hsieh and W.-H. Tuan, *Mater. Sci. Eng., A*, **425**, 349 (2006).
35. W. D. Callister, *Materials Sciense and Engineering: An Introduction*, John Wiley & Sons, (1996).
36. Y. Woo and S.-H. Kim, *J. Mater. Sci. Technol.*, **25**, 1017 (2011).